

## Article

# Experimental Study on Mechanical Properties of Structured Clay under Different Unloading Rates and Unloading Stress Paths

Lu Li, Meng Zang \*, Rongtang Zhang and Haijun Lu

School of Civil Engineering and Architecture, Wuhan Polytechnic University, Wuhan 430023, China

\* Correspondence: zangmeng@whpu.edu.cn

**Abstract:** Consolidated undrained triaxial shear tests were performed on undisturbed saturated structured clay at three unloading rates (0.1, 0.25, and 2.5 kPa/min) using a GDS triaxial system to determine the effects of different unloading rates and unloading stress paths on the stress–strain relationship, pore pressure variation, and failure strength characteristics of Zhanjiang structured clay. Microstructural changes in the clay were observed during shear tests at different unloading rates. Furthermore, the obtained stress–strain relationship indicates strain-softening under different unloading stress paths. Under the same axial strain, a larger unloading rate caused a larger deviatoric stress. Under the same conditions, the higher the confining pressure, the greater the peak pore pressure, the smaller the unloading rate, the greater the pore pressure development, and the greater the variation in the pore pressure. Moreover, the undrained shear strength increased with an increase in the unloading rate from 0.1 to 2.5 kPa/min. The change in the unloading rate had a greater effect on the undrained strength under the passive tensile path than that under the passive compression path. The microstructure of the Zhanjiang structured clay changed after shear tests at different unloading rates, exhibiting various degrees of adjustment in the particle arrangement, contact relations, pore sizes, and shapes.



**Citation:** Li, L.; Zang, M.; Zhang, R.; Lu, H. Experimental Study on Mechanical Properties of Structured Clay under Different Unloading Rates and Unloading Stress Paths. *Buildings* **2023**, *13*, 1544. <https://doi.org/10.3390/buildings13061544>

Academic Editors: Erwin Oh, Yongqiang Zhou, Erdi Abi, Longlong Lv and Shaobo Chai

Received: 17 May 2023

Revised: 4 June 2023

Accepted: 15 June 2023

Published: 17 June 2023



**Copyright:** © 2023 by the authors. Licensee MDPI, Basel, Switzerland. This article is an open access article distributed under the terms and conditions of the Creative Commons Attribution (CC BY) license (<https://creativecommons.org/licenses/by/4.0/>).

**Keywords:** structured clay; unloading stress path; unloading rate; unloading failure strength

## 1. Introduction

The mechanical properties of soft clay, such as deformation and strength, are related to stress paths [1,2] and corresponding rate effects [3–5] owing to the characteristics of high clay grain content, high moisture content, and large pore ratio, among others. The excavation of a foundation pit is a typical unloading project in geotechnical engineering. The deformation characteristics, mechanical parameters, and failure mechanisms of soils significantly differ when they undergo different unloading stress paths and unloading rates to reach the same stress state [6].

Numerous studies on the mechanical properties of soils under unloading stress paths have been conducted, and remarkable achievements have been made. Liu et al. [7] demonstrated that the stress–strain relationship for soft soils is affected by unloading stress paths. Yan et al. [8] found that excess pore pressure in saturated soft clay under unloading conditions effects the excavation of foundation pit and heave of pit bottom through a comparative study between triaxial unloading experiments and theoretical research. Lim et al. [9] demonstrated that the unloading mechanical parameters of soft soils can be used to accurately calculate the excavation deformations of foundation pits under undrained conditions. Huang et al. [1] conducted  $K_0$  consolidation undrained shear tests on Shenzhen soft soil under the influence of unloading stress paths; the results showed variation in the unloading strength and initial shear modulus of soils under unloading stress paths, and the deformation properties of soils were greatly influenced by the unloading stress paths. Jia et al. [10] performed axial loading and lateral unloading shear tests on Wenzhou soft

clay using a stress-path triaxial apparatus and proposed a four-parameter stress–strain curve model based on the deformation mechanism of structured soils and incremental linear elasticity theory. Huang et al. [11] reported that the unloading strength parameters and unloading modulus of marine sedimentary soft soils were significantly influenced by the unloading stress paths, and an increase in excess pore water pressure weakened the unloading strengths, particularly when the cohesion was stronger. The above studies indicate that mechanical properties including the stress–strain relationship, pore pressure characteristics, deformation and strength characteristics at failure, and the initial unloading modulus of soils are significantly related to the unloading stress paths.

In the 1930s, Buisman [12] reported that the stress, strain, and strength of soils exhibited a non-negligible rate-dependent relationship via indoor experiments. Some researchers have conducted rate-dependent tests on different clays [13–15] and concluded that the undrained shear strength increases with increasing strain rates, thus considering the shear strength rate parameters for quantitative description. For example, Whitman et al. [14] obtained the strength rate parameter of 3.5% for Mississippi alluvial soils, but the magnitude of the effects of the increasing strain rate on the undrained shear strength varied greatly. Zhu et al. [15] performed shear tests on saturated marine clay under compression and tension path conditions at three different strain rates and found that the effect of the shear rate on the undrained shear strength of the tension path was greater than that of the compression path. Wu et al. [16] conducted  $K_0$ -consolidation undrained triaxial tests on marine clay considering the effects of stress states and strain rates and concluded that the higher the strain rate, the higher the undrained shear strength, and the lower the pore pressure of soils with different over-consolidation ratios. Cai's [17] research results demonstrated that strong structured clay presents a unique shear rate mechanical effect, and its consolidation undrained shear strength does not change monotonically with shear rate but is characterized by first decreasing and then increasing with increasing shear strain rate, and there is a critical rate phenomenon. These previous research outcomes indicate that the strength characteristics of soils are strongly related to the shear rate. However, these tests generally examined the strain rate effects under a specific stress history, which is not entirely applicable to actual excavation projects, such as those involving slopes and foundation pits, where stress rate problems exist. Meanwhile, Li et al. [18] analyzed the mechanical properties of undisturbed expansive clay under the influence of different unloading rates and unloading stress paths using a GDS stress-path triaxial apparatus. The results showed that the pore pressure of soils under reduced compression and reduced extension stress paths remained negative, the undrained shear strength increased with an increase in unloading rate, and the failure pattern of expansive clay was related to the shear rate and microcracks. Yang et al. [19] performed undrained unloading tests of isotropic consolidation on a soft dredger fill and developed formulas for the initial tangent modulus and unloading failure strength considering the influence of the unloading rates and unloading stress paths. Song et al. [20] conducted triaxial tests on remolded deep clay under the effect of stress paths and stress rates. As a result, the strength of soils exhibited a strong rate dependence under different stress paths, and the damage caused by unloading conditions on soil was more abrupt than that caused by loading conditions.

The aforementioned studies comprehensively considered the influence of unloading stress paths and unloading rates on the mechanical properties of soils; however, most focused on soft soils with weak structural properties. Zhanjiang clay is known for its strong structural properties, with an open flocculation structure and strong cementation of free oxides at the microscopic level, as well as an abnormal combination of poor physical properties and good mechanical property indices at the macroscopic level. To date, a certain understanding of the static and dynamic properties as well as microscopic mechanisms of Zhanjiang clay has been achieved [21–24], whereas the mechanical properties of strong structured clay under the influence of different unloading stress paths and unloading rates are less researched. Therefore, in this study, a series of undrained unloading tests was conducted under isotropic consolidation conditions regarding various unloading stress paths

and unloading rates to simulate different unloading methods and speeds in foundation pit excavation projects as well as to investigate the influence law of different unloading stress paths and unloading rates on the strain, pore pressure, and strength characteristics of strong structured clay, with the aim of providing a reference and theoretical basis for the selection of geotechnical engineering parameters in structured clay areas.

## 2. Materials and Methods

### 2.1. Test Material

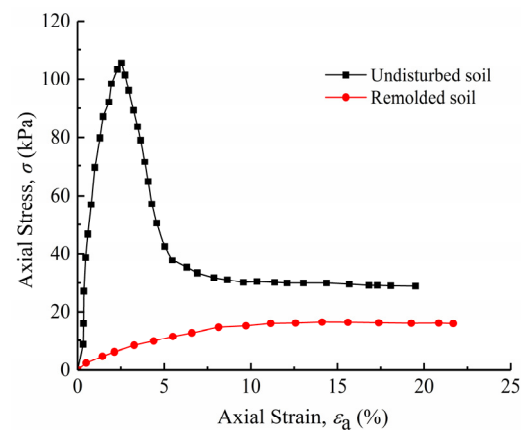
Test soil samples were obtained from the foundation pit in Zhanjiang City (Figure 1), at the depth of 8–10 m. The soil sample was grey-brown and homogeneous, and the horizontal (normal) direction had weak laminar surface development. The physical and mechanical indices of the test soil samples are presented in Table 1; the moisture content, particle density, liquid and plastic limits, and permeability test were determined as per ASTM D2216-19, ASTM D854-92, ASTM D4318-17e1, and ASTM D1586-11, respectively [25–28], indicating that the Zhanjiang clay possesses inferior physical properties, such as high natural moisture content, large void ratio, high liquid–plastic limit, and small vertical permeability coefficient, but superior mechanical properties, including high unconfined compressive strength. The results of the unconfined compressive strength tests on undisturbed and remolded Zhanjiang clay are displayed in Figure 2, the results were determined as per ASTM D2166-16 [29], and the unconfined compressive strengths of undisturbed soil and remolded soil were 114 and 16.4 kPa, respectively, with the sensitivity of 6.95. According to the classification suggested by Touiti et al., Zhanjiang clay should be considered a medium-sensitive clay [30]. Undisturbed Zhanjiang soil samples exhibit significant brittleness characteristics, as deformation was observed under compression and the peak stress was realized at small axial strain; with the apparent failure surface, the soil sample resistance decays rapidly. The strength of the remolded soil gradually increases with the development of deformation and eventually results in ductile bulging failure [24].



Figure 1. Sampling location in Zhanjiang City, Guangdong Province, China.

Table 1. Physical and mechanical indices for Zhanjiang structured clay.

Particle Density/(g·cm <sup>-3</sup> )	Moisture Content w/%	Liquid Limit w <sub>L</sub> /%	Plastic Limit w <sub>p</sub> /%	Plasticity Index I <sub>p</sub>	Void Ratio e <sub>0</sub>	Vertical Permeability Coefficient K/(10 <sup>-7</sup> cm/s)	Unconfined Compressive Strength q <sub>u</sub> /kPa	Structural Yield Stress σ <sub>k</sub> /kPa
2.69	43.85	54.2	20.8	33.4	1.2	2.6	114	300–400



**Figure 2.** Unconfined compressive stress–strain curve for Zhanjiang structured clay.

The X-ray diffraction (XRD) results of the Zhanjiang structured clay are presented in Figure 3 and Table 2. Clay minerals (<0.005 mm) accounted for more than 60% of the particle composition; therefore, the Zhanjiang clay was classified as soft clay.

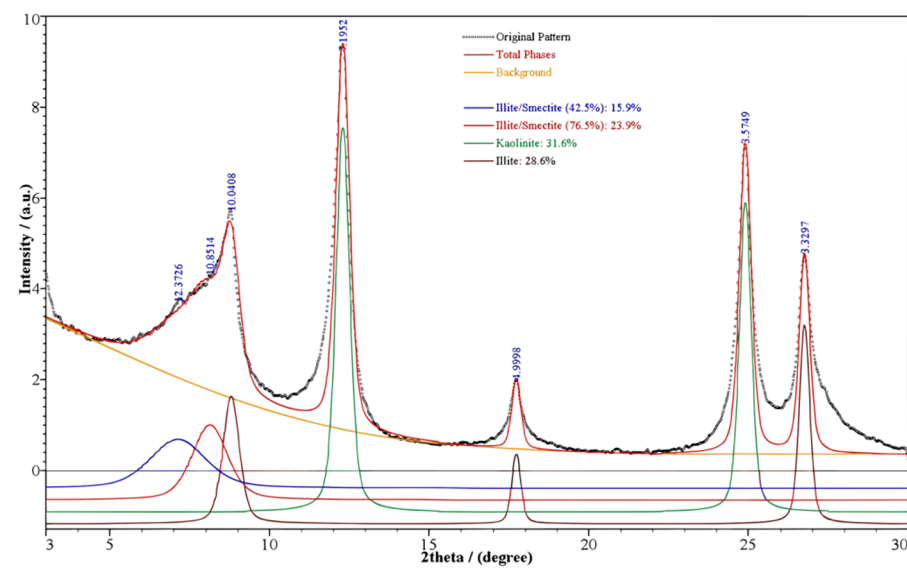


**Figure 3.** XRD result for Zhanjiang structured clay.

**Table 2.** Mineral composition of Zhanjiang structured clay.

Relative Mineral Content/%						
Quartz	K-Feldspar	Na-Feldspar	Illite	Kaolinite	Illite-Smectite Mixed LayerI	Illite-Smectite Mixed LayerII
62	3	3	8.96	10.24	5.12	7.68

## 2.2. Determination of Unloading Stress Path

The stress paths experienced by the soil in various parts during the excavation of a foundation pit are complex and vary significantly with excavation depth, excavation method, and support form of the foundation pit. In this study, four stress paths were considered, experienced by the soil in typical parts (A, B, and C) of the active and passive zones of the pit, and employed as the test paths, as depicted in Figure 4.

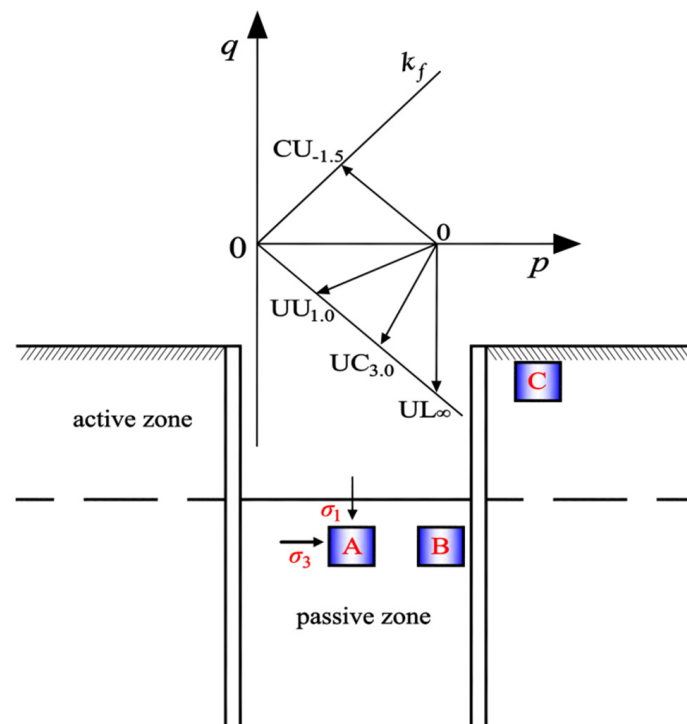


**Figure 4.** Schematic of soil stress states and unloading stress paths in foundation pit projects.

In the passive earth pressure zone, for soil unit A near the excavation surface of the foundation pit, the vertical unloading is the most obviously affected by the excavation of the overlying soils. This indicates that the axial stress unloading and the horizontal stress remain unchanged ( $\sigma_1$  decreases,  $\sigma_3$  remains unchanged), so the unloading stress path expressed as UC<sub>3.0</sub> and the horizontal stress may decrease with uplifting of the pit bottom. In addition, there will be both the axial stress and horizontal stress unloading ( $\sigma_1$  decreases,  $\sigma_3$  decreases), so the unloading stress path is expressed as UU<sub>1.0</sub>. Furthermore, offset of the foundation pit support into the pit can lead to the axial stress unloading and the horizontal stress loading ( $\sigma_1$  decreases,  $\sigma_3$  increases) of soil unit B, and the unloading stress path is expressed as UL <sub>$\infty$</sub> . In the active earth pressure zone, with the excavation of the foundation pit, the horizontal stress decreases and the axial stress remains unchanged ( $\sigma_3$  decreases,  $\sigma_1$  remains unchanged) for the soil on the outside of the foundation support, i.e., soil unit C; the unloading stress path is expressed as CU<sub>-1.5</sub>. Accordingly, four representative unloading paths were selected: UC<sub>3.0</sub>, UU<sub>1.0</sub>, UL <sub>$\infty$</sub> , and CU<sub>-1.5</sub>. The stress paths were named as L for loading, C for constant load, U for unloading, and the former letter for the vertical stress state, the latter letter for the horizontal stress state, and the footnote for the stress path slope  $\eta = \Delta q / \Delta p$  [23].

### 2.3. Selection of Unloading Rate

During the excavation of a foundation pit, the mechanical properties of soils are influenced by not only the stress path, but also the speed of excavation (i.e., different unloading rates), particularly the strength and deformation properties of the soil. In this study, we initially set several groups of different unloading rates based on various unloading stress paths through indoor tests. The specific unloading rate selection scheme is shown in Table 3.

**Table 3.** Preliminary selection scheme for unloading rates.

Group	Unloading Rate, $v/\text{kPa}\cdot\text{min}^{-1}$	Confining Pressure/ $\text{kPa}$	Unloading Stress Path
I	0.01, 0.025, 0.05	100	UC <sub>3.0</sub> ( $\sigma_1$ decreases, $\sigma_3$ remains unchanged)
II	0.25, 0.5, 1	100	UC <sub>3.0</sub> ( $\sigma_1$ decreases, $\sigma_3$ remains unchanged)
III	0.1, 0.25, 2.5	100	UC <sub>3.0</sub> ( $\sigma_1$ decreases, $\sigma_3$ remains unchanged)

The stress–strain relationship curves obtained from the test scheme in Table 3 are shown in Figure 5.

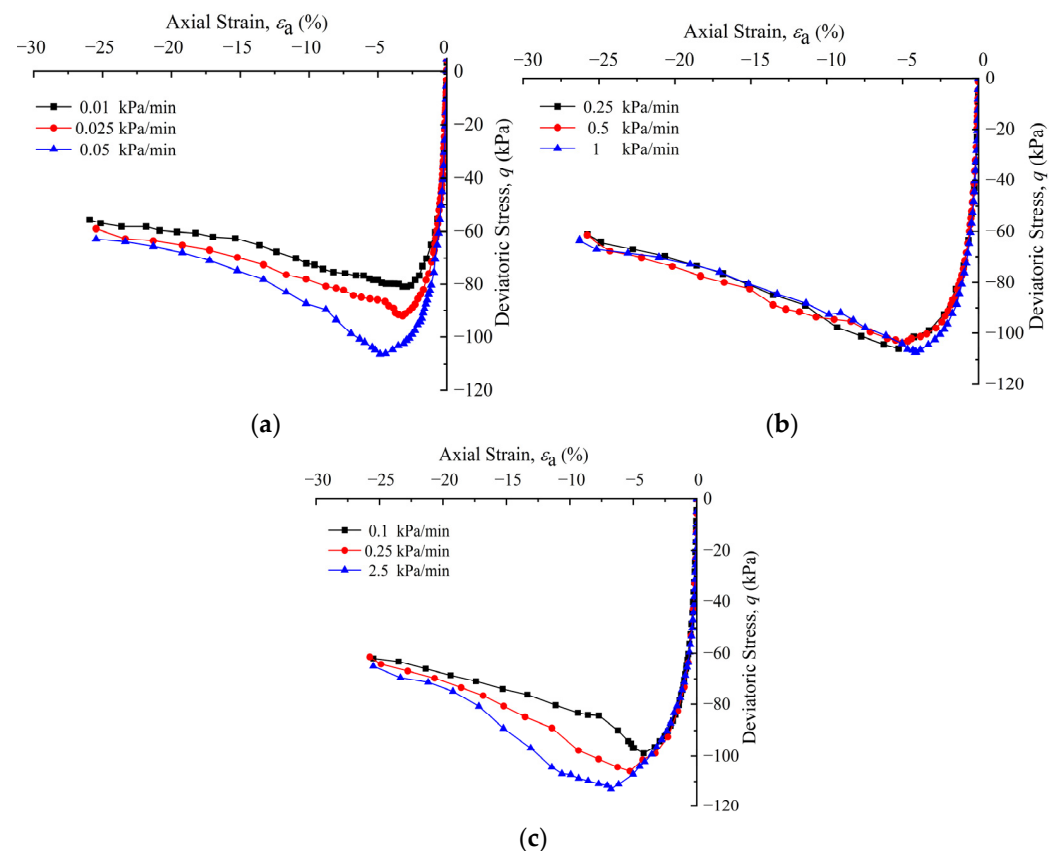


**Figure 5.** Stress–strain curves obtained under different unloading rates. (a) I: 0.01, 0.025, 0.05  $\text{kPa}\cdot\text{min}^{-1}$ ; (b) II: 0.25, 0.5, 1  $\text{kPa}\cdot\text{min}^{-1}$ ; (c) III: 0.1, 0.25, 2.5  $\text{kPa}\cdot\text{min}^{-1}$ .

From Figure 5, it can be seen that the stress–strain relationship curves for the Zhanjiang structured clay under different unloading rates exhibit strain softening. In the cases of unloading rates of 0.01, 0.025, 0.05  $\text{kPa}/\text{min}$  and 0.25, 0.5, 1  $\text{kPa}/\text{min}$ , the stress–strain curves corresponding to 0.25, 0.5, and 1  $\text{kPa}/\text{min}$  are not sensitive to this unloading rate. Therefore, the unloading rate is insignificant in engineering practice and was not examined further in this study. Since a foundation pit project generally requires rapid excavation and support, and the soil experiences the unloading stress path predominantly under undrained conditions, the final unloading rates were taken as 0.1, 0.25, and 2.5  $\text{kPa}/\text{min}$  considering the test period and the actual excavation rate of the foundation pit project. The experimental scheme is summarized in Table 4.

**Table 4.** Unloading rate test programs.

Zone	Consolidation Confining Pressure/kPa	Stress Path Slope/ $\eta$	Unloading Stress Path	Unloading Rate $v/\text{kPa}\cdot\text{min}^{-1}$	Drainage Condition
Active earth pressure zone	50/100/200	-1.5	CU <sub>-1.5</sub> ( $\sigma_1$ remains unchanged, $\sigma_3$ decreases)	0.1, 0.25, 2.5	Undrained
Passive earth pressure zone	50/100/200	1.0	UU <sub>1.0</sub> ( $\sigma_1$ decreases, $\sigma_3$ decreases)	0.1, 0.25, 2.5	
		3.0	UC <sub>3.0</sub> ( $\sigma_1$ decreases, $\sigma_3$ remains unchanged)		
		$\infty$	UL <sub><math>\infty</math></sub> ( $\sigma_1$ decreases, $\sigma_3$ increases)		

#### 2.4. Test Method

The test apparatus was a GDS stress-path triaxial apparatus, and the specimen was trimmed using a wire saw, which was a cylinder with a height of 80.0 mm and diameter of 39.1 mm. The specimen encased in the rubber membrane was sealed at the cap (the receiving element) and base (the transmitting element) and positioned in a triaxial compression chamber, after which pressure was applied. Vacuum suction saturation and back pressure saturation were prepared before testing, and an undrained triaxial shear test was performed according to the set stress path after isotropic consolidation. The test was completed when the axial strain reached 20%, and the test results were determined according to ASTM D4767-11 [31].

### 3. Results and Discussion

There are two types of specimen failures under unloading conditions: compression and elongation failures. The analysis shows that among the four stress paths in Table 4, the failure mode of the specimen under CU<sub>-1.5</sub> path is axial compression failure, while that of the specimen under the other three stress paths is axial elongation failure, or “tensile failure”. The failure modes of specimens are provided in Figure 6.

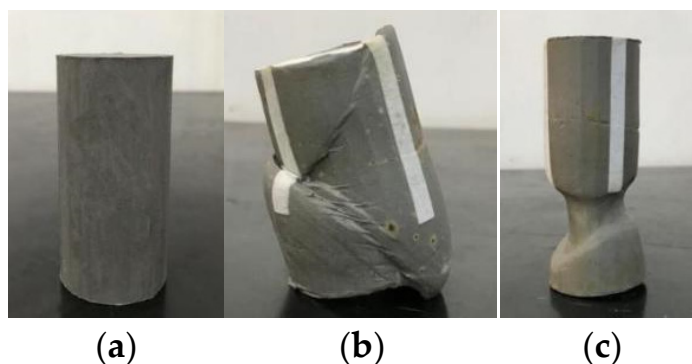


**Figure 6.** Typical failure modes of specimens. (a) Undisturbed sample before test; (b) compression failure; (c) tensile failure.

#### 3.1. Effect of Unloading Rate on Stress-Strain Relationship

The deviatoric stress–axial strain curves for the Zhanjiang structured clay under different unloading stress paths are shown in Figures 7–10. Deviatoric stress  $q = \sigma_1 - \sigma_3$ : in the passive compression path,  $q$  is positive (CU<sub>-1.5</sub>); in the passive tensile paths,  $q$  is negative (UC<sub>3.0</sub>, UL <sub>$\infty$</sub> , UU<sub>1.0</sub>), while the axial strain is positive in the compression path and negative in the tensile path.

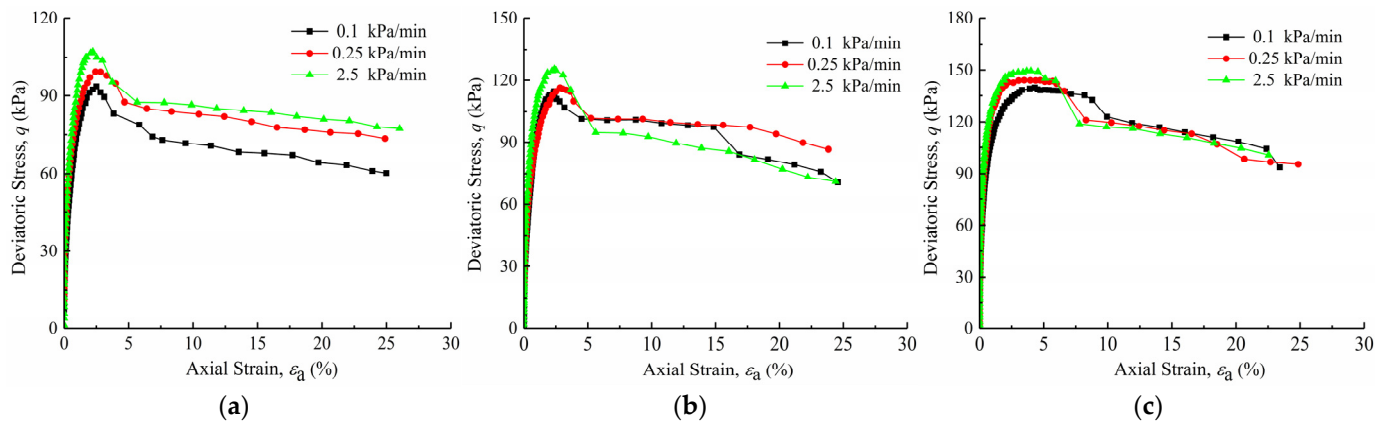


**Figure 7.** Strain–stress curves for  $CU_{-1.5}$  path under different confining pressure. (a) 50 kPa; (b) 100 kPa; (c) 200 kPa.

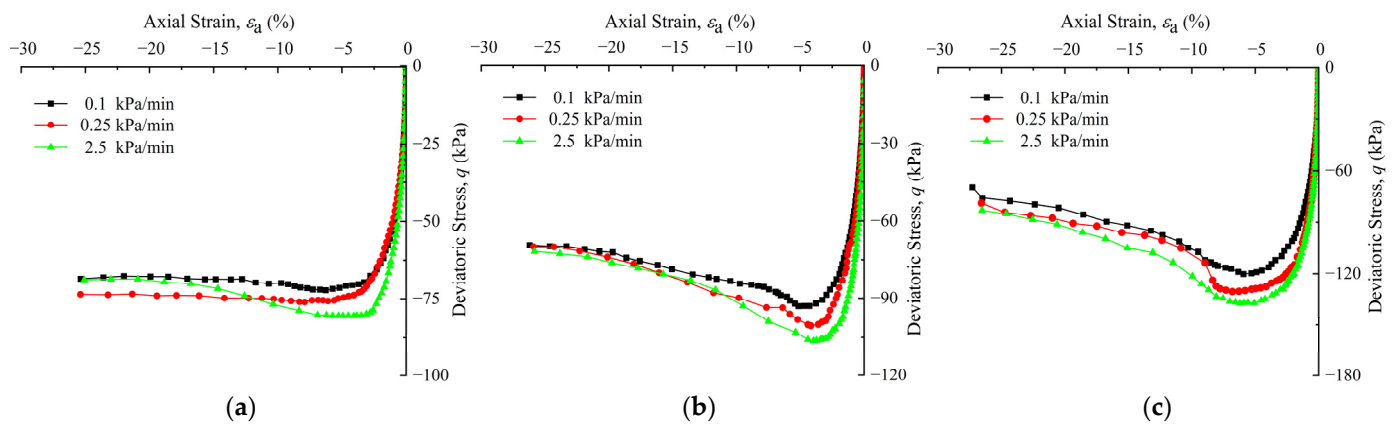


**Figure 8.** Strain–stress curves for  $UU_{1.0}$  path under different confining pressure. (a) 50 kPa; (b) 100 kPa; (c) 200 kPa.

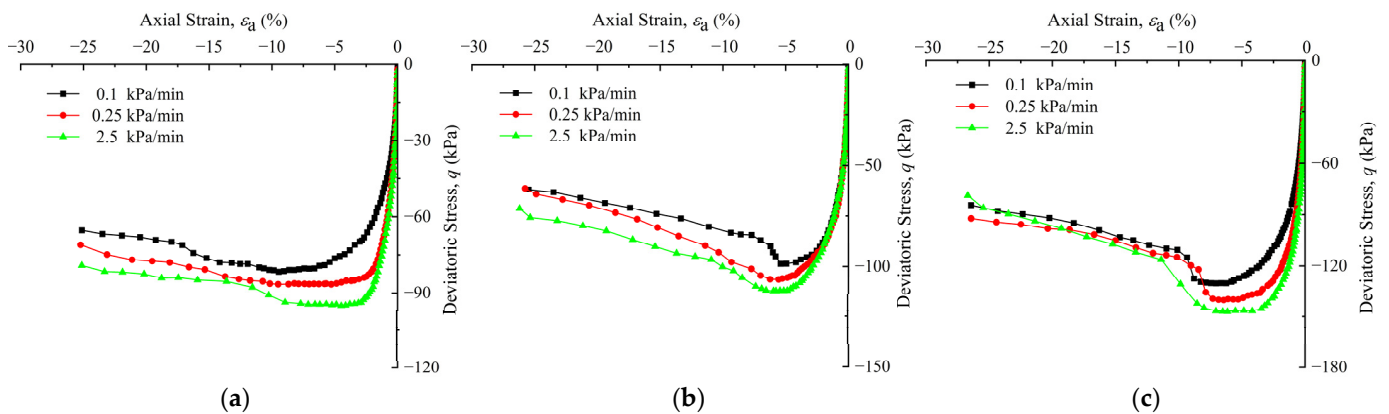


**Figure 9.** Strain–stress curves for  $UC_{3.0}$  path under different confining pressure. (a) 50 kPa; (b) 100 kPa; (c) 200 kPa.

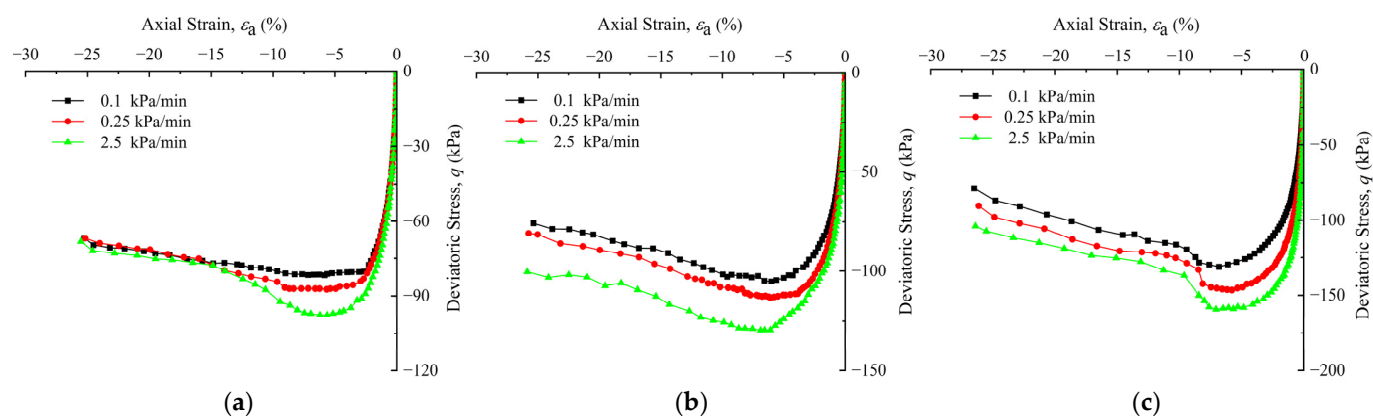


**Figure 10.** Strain–stress curves for  $UL_{\infty}$  path under different confining pressure. (a) 50 kPa; (b) 100 kPa; (c) 200 kPa.

From Figures 7–10, it can be seen that the stress–strain curves for Zhanjiang structured clay exhibit strain softening at different unloading rates under both passive compression and passive tensile paths; more specifically, with an increase in axial strain, the deviatoric stress first increases rapidly and then gradually decreases after reaching the peak stress. Under the passive compression path, the smaller the confining pressure, the more significant the strain softening; whereas, under the passive tensile path, the larger the confining pressure, the more evident the strain softening. For the same axial strain, the larger the unloading rate, the greater the deviatoric stress of the soil under the same unloading stress path; further, with increased unloading rate, the soil obtained a higher secant modulus, which decreased significantly with increase in unloading time. Therefore, quick excavation with instantly available support is advisable during corresponding construction.

Under the same stress path and confining pressure, the stress–strain curves for the specimen at different unloading rates are more concentrated in the initial stage of unloading, at low deviatoric stress and soil deformation, demonstrating that the stress–strain curves were not sensitive to the unloading rate at this stage. Moreover, with an increase in the unloading amount, when the deviatoric stress reaches the failure stress of the soil and the strain increases rapidly, the soil undergoes large deformation failure, and the strength of the soil decays rapidly. Furthermore, for the same consolidation pressure, the peak deviatoric stress of the stress–strain curves is related to the unloading rate; the larger the unloading rate, the larger the failure stress of the soil. This is because when the unloading rate is high, the soil particles do not have enough time to move during shearing, and it is difficult to overcome the slip, rotation, rolling, and transposition resistance between particles in a relatively short period. Only when the energy gathers to the effective stress then the resistance of the particles is overcome, forming a dislocation and producing deformation, which resulted in large macroscopic failure stress. When the unloading rate is low, the soil particles have more time for directional adjustment or displacement in the longer unloading period to achieve rolling and directional arrangement of the particles; thus, the failure stress was smaller.

The stress–strain curves under the  $CU_{-1.5}$  unloading path clearly differ from those for the other three groups of stress paths. The deformation of the specimen under the  $CU_{-1.5}$  path exhibited axial compression, and the axial strain when the specimens reached failure was between 2% and 4%. In foundation pit excavation projects, the soil outside the foundation pit support in the active earth pressure zone is damaged when a small strain is generated. This indicates that the soil outside the pit can reach the active limit equilibrium state under a small lateral deformation. Therefore, the horizontal displacement of the retaining wall should be effectively controlled in actual engineering to avoid sliding damage to the soil behind the retaining wall. Furthermore, the deformation of the specimens under the  $UC_{3.0}$ ,  $UL_{\infty}$ , and  $UU_{1.0}$  paths showed axial elongation, and the axial strains when the specimens reached failure under the passive tensile paths were mostly concentrated around

4~9%. In actual engineering, soil uplift deformation at the bottom of the pit should be monitored to avoid soil uplift damage in the foundation pit, i.e., the strain of the soil inside the foundation pit in the passive earth pressure area is larger when damage is produced.

### 3.2. Effect of Unloading Rate on Pore Water Pressure

The pore pressure–strain relationship curves of the specimens under different unloading paths are displayed in Figures 11–14. It can be seen from the figures that the confining pressure influences the development of pore pressure: under the same conditions, the larger the confining pressure, the larger the peak pore pressure or the final pore pressure value. The change law for the pore pressure with strain is the result of the combined effect of the pore pressures generated by elastic expansion and plastic deformation during shearing.

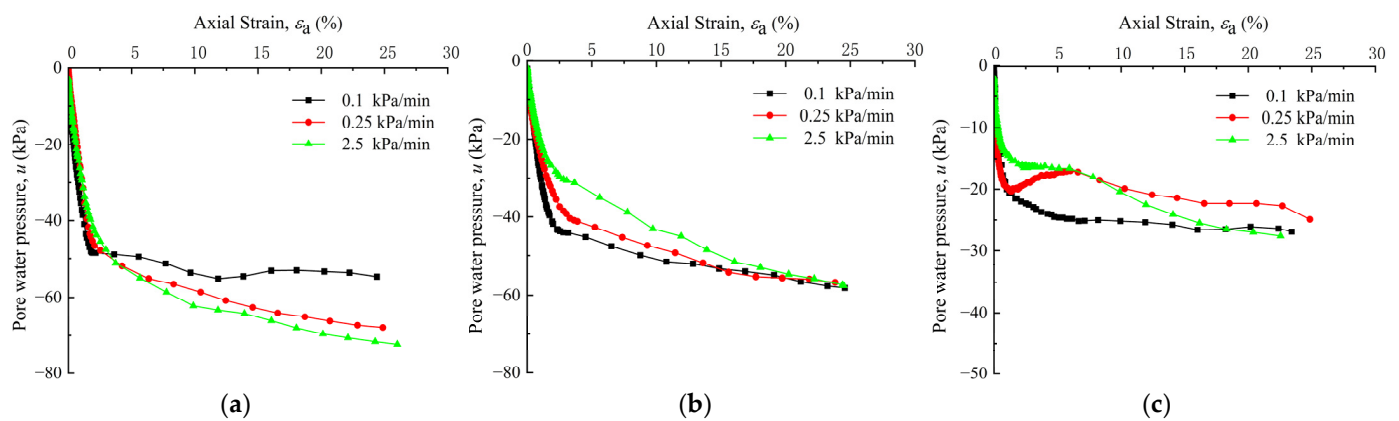


**Figure 11.** Pore pressure–strain curves for  $CU_{-1.5}$  path under different confining pressure. (a) 50 kPa; (b) 100 kPa; (c) 200 kPa.

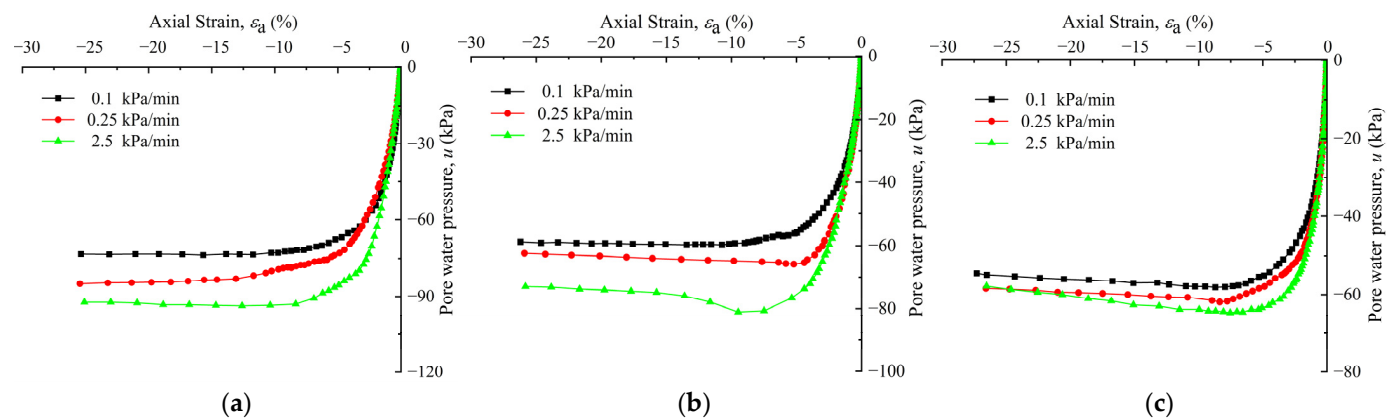


**Figure 12.** Pore pressure–strain curves for  $UU_{1.0}$  path under different confining pressure. (a) 50 kPa; (b) 100 kPa; (c) 200 kPa.

The pore water pressure change laws are quite different under various stress paths. Under the  $CU_{-1.5}$  passive compression path, the pore water pressure remained negative with the development of strain. At the beginning of unloading, the pore water pressure accumulated rapidly with an increase in tensile strain, and after the strain exceeded a certain value, the growth of the negative pore water pressure gradually slowed. This is because the negative pore water pressure generated by the elastic expansion at the beginning of unloading was greater than the positive pore water pressure generated by the unloading compression. Thus, the pore water pressure decreased rapidly, and with the increase in the deviatoric stress, the growth rate of the pore water pressure generated by the elastic expansion and plastic deformation of the soil slowed, and the pore water pressure tended to a stable state. Moreover, under the same conditions, the larger the unloading rate, the

slower the pore water pressure development at the beginning of unloading. This is because, in the initial stage of unloading, the faster the unloading speed, the less time the pore water pressure generated by elastic expansion has to grow. As the unloading continued, the failure stress of the soil increased, and the final pore water pressure increased.

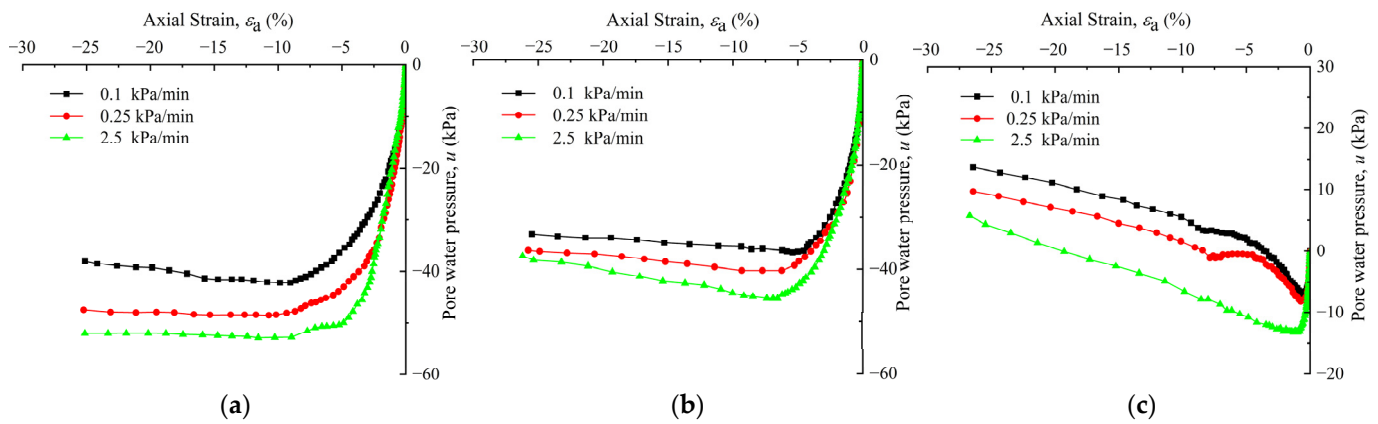


**Figure 13.** Pore pressure–strain curves for UC<sub>3,0</sub> path under different confining pressure. (a) 50 kPa; (b) 100 kPa; (c) 200 kPa.

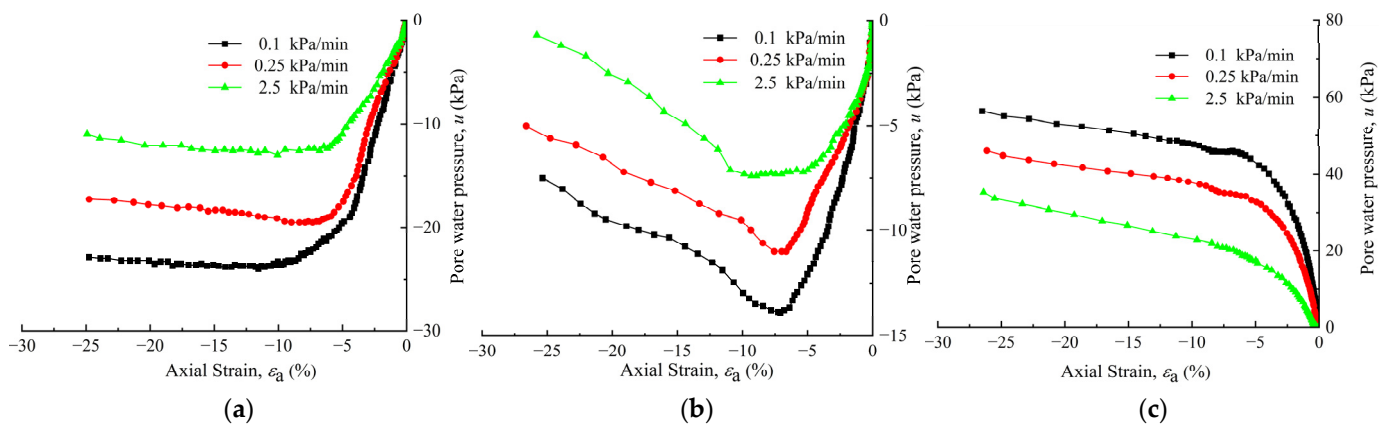


**Figure 14.** Pore pressure–strain curves for UL<sub>∞</sub> path under different confining pressure. (a) 50 kPa; (b) 100 kPa; (c) 200 kPa.

Under the UU<sub>1,0</sub> passive tensile path, the development law for the pore water pressure with axial strain during shearing under different confining pressures is essentially the same. Moreover, the pore water pressure generated during the entire unloading process remained negative, and the pore water pressure decreased rapidly with the increase in axial strain, then slowed and gradually stabilized. This is due to the unloading of the lateral stress. The soil sample will have a certain degree of elastic expansion and the pore water pressure will decrease, which will be influenced by the axial stress. Specifically, when the unloading stress path is UU<sub>1,0</sub>, both the axial and lateral stresses decreased throughout the shearing process; thus, the pore water pressure decreased significantly and remained negative.

Under the UC<sub>3,0</sub> and UL<sub>∞</sub> passive tensile paths, when the confining pressure was small, i.e., 50 and 100 kPa, the negative pore water pressure first increased and then decreased with increasing axial strain during the shearing process. Before reaching the yield point of the soil, the negative pore water pressure generated by the elastic expansion was larger than the positive pore water pressure generated by the plastic deformation; therefore, the pore water pressure first decreased rapidly and then gradually increased, owing to the deviatoric stress. After reaching the yield point, the pore water pressure generated by the plastic deformation caused by the shearing failure gradually became larger than that

generated by the elastic expansion. Thus, the pore water pressure increased rapidly, and the pore water pressure–strain curves exhibit a corresponding turning point. Moreover, when the confining pressure was larger (e.g., 200 kPa), the pore water pressure of the specimens changed from negative to positive. The negative pore water pressure generated by the elastic expansion was smaller than the positive pore water pressure generated by the plastic deformation during shearing, and the pore water pressure tended to increase monotonically with the axial strain. Furthermore, the smaller the unloading rate under the same conditions, the more fully the pore pressure develops, and the greater the pore pressure variation.

In summary, during the unloading process, the negative pore pressure gradually increased at the start of unloading, and the axial strain varies when the pore pressure reached its maximum value under different unloading paths. The unloading rate affected the growth path and dissipation rate of negative pore pressure. Owing to the high moisture content and low permeability coefficient of the soft clay, the unloading of the pit excavation will generate a negative excess pore pressure in the pit bottom and surrounding soil. With the dissipation of the negative pore pressure, the effective stress in the soil at the bottom of the pit gradually decreases, which then causes the expansion and uplift of the soil at the bottom of the pit. Therefore, during the unloading construction, attention should be paid to engineering disasters caused by negative pore water pressure dissipation.

### 3.3. Effect of Unloading Rate on Stress Path

The total and effective stress paths of the Zhanjiang structured clay under different unloading paths are depicted in Figures 15–18. It can be seen from the figures that when the unloading path is the same, the change trends of the total stress paths under different consolidation pressures are basically the same, and all of them develop according to the stress path in the set  $p$ - $q$  plane. The test consistency was good, indicating that the results of this experiment were reliable. Additionally, the development laws for the effective stress paths of the Zhangjiang structured clay under different unloading rates are essentially the same. In the initial shearing, the effective stress path was linear, and the difference in the stress rate was manifested in the stress path by the different ratios of  $dq/dp'$ , which was at the stage of a large increase in the deviatoric stress in the smaller strain range of the stress–strain curves. Due to the low permeability of clay, there is hysteresis in the growth of the pore water pressure, resulting in small differences in the pore water pressure at different unloading rates; therefore, the effective stress paths overlap in the initial stage of shearing. As shearing continued, the pore water pressure in the specimen began to increase rapidly; therefore, the effective stress path and the total stress path at different stress paths began to separate. Moreover, with decreases in the unloading rate, the deflection range of the effective stress path became continually larger, which coincides with the largest variation range in the pore pressure at the unloading rate of 0.1 kPa/min in the pore water pressure and strain relationship graph.

The effective stress path of the specimen under the CU<sub>-1.5</sub> and UU<sub>1.0</sub> unloading stress paths remains on the right side of the total stress path, which is because the pore water pressure of the specimens under these paths is always negative. Additionally, under the UC<sub>3.0</sub> and UL<sub>∞</sub> unloading stress paths, the pore water pressure of the specimens is negative at small confining pressure, and the effective stress path is on the right side of the total stress path; however, when the confining pressure is large, the pore water pressure changes from negative to positive with development of the axial strain, and the effective stress path gradually inclines from the right side to the left side.

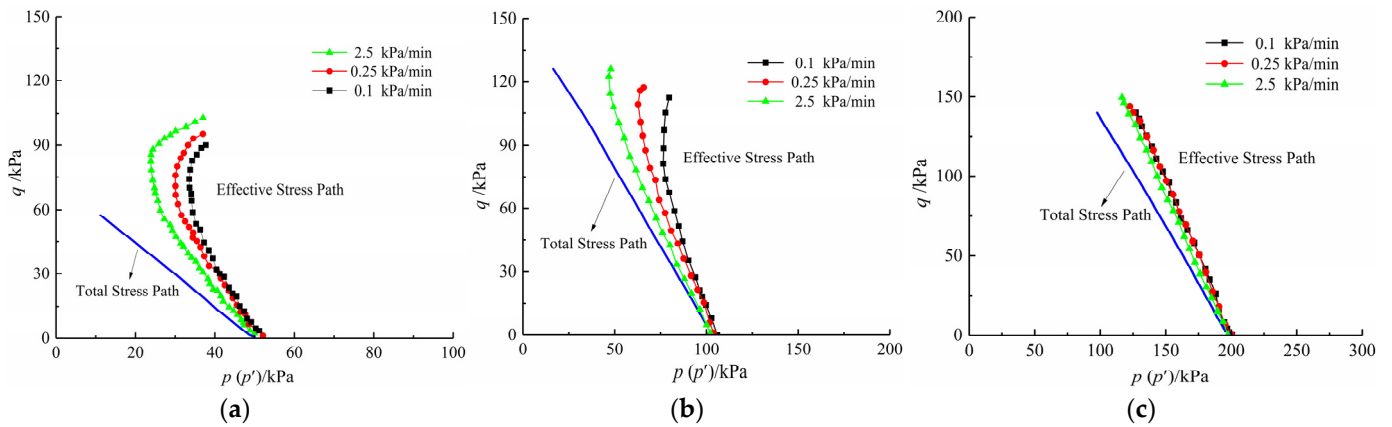


**Figure 15.** Effective stress path and total stress path under  $CU_{-1.5}$  path for different confining. (a) 50 kPa; (b) 100 kPa; (c) 200 kPa.

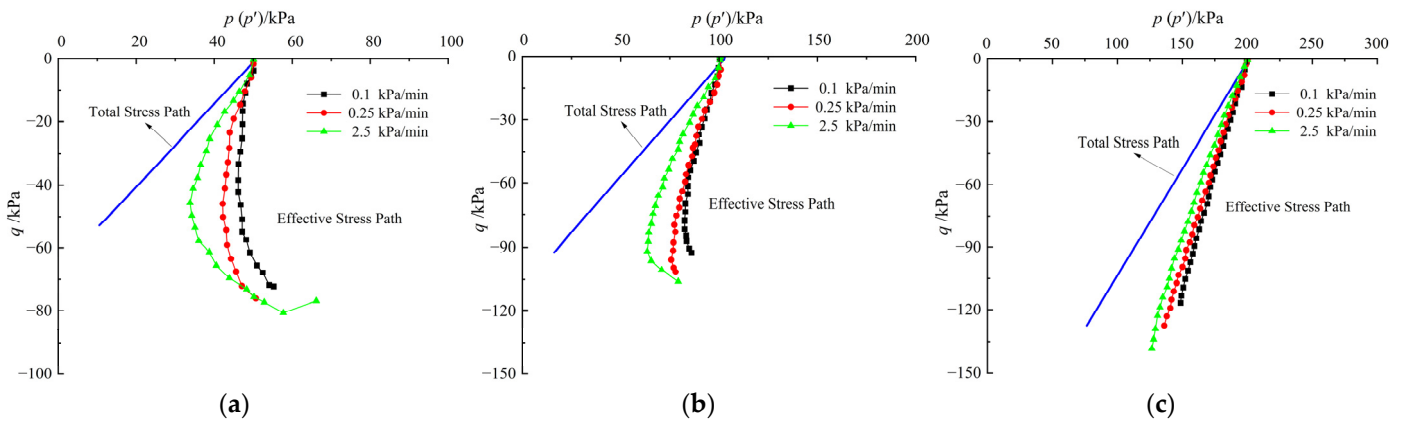


**Figure 16.** Effective stress path and total stress path under  $UU_{1.0}$  path for different confining. (a) 50 kPa; (b) 100 kPa; (c) 200 kPa.

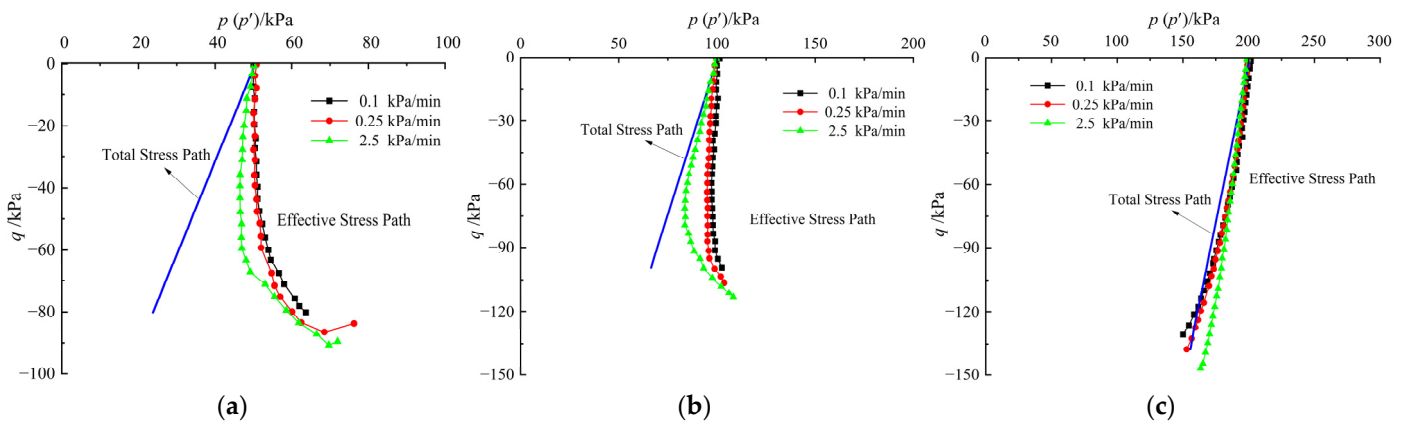


**Figure 17.** Effective stress path and total stress path under  $UC_{3.0}$  path for different confining. (a) 50 kPa; (b) 100 kPa; (c) 200 kPa.

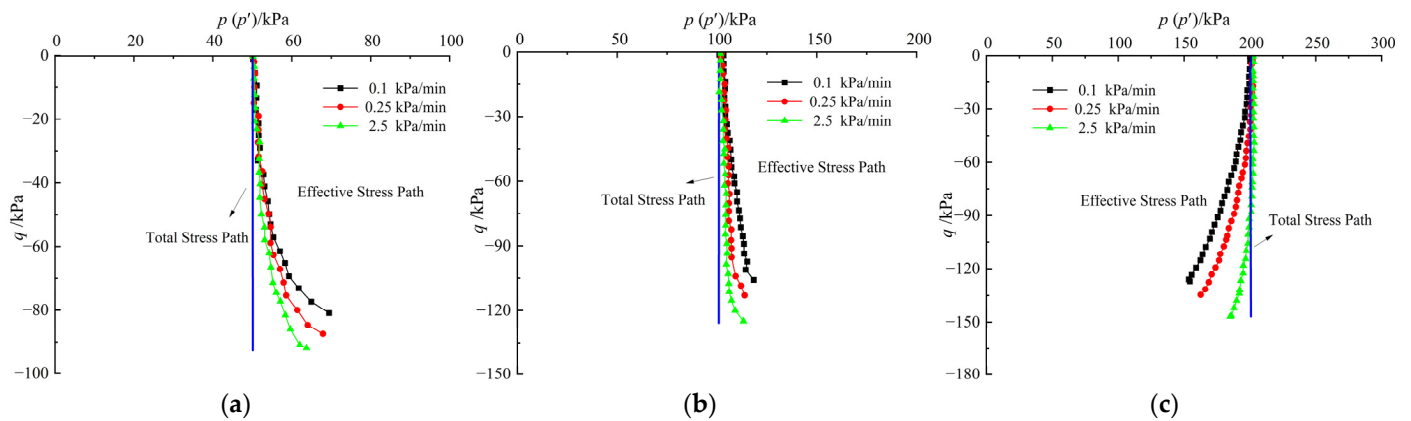


**Figure 18.** Effective stress path and total stress path under  $UL_{\infty}$  path for different confining pressure. (a) 50 kPa; (b) 100 kPa; (c) 200 kPa.

### 3.4. Expressions for Unloading Rate Parameters

The relationship curves for the failure strength and unloading rate of specimens under different unloading paths are presented in Figure 19. It can be observed from the figures that the unloading strength of the specimens varies in magnitude at different consolidation pressures, and the larger the confining pressure, the greater the influence of the unloading rate on the unloading strength of the soil. The unloading strength of the soil under the  $UU_{1.0}$  unloading path was the smallest, followed by that under  $UC_{3.0}$ , and the largest was under the  $UL_{\infty}$  path. Additionally, under the same unloading path, the failure strength of the soil increased with increasing unloading rate, and the failure strength of the soil increased more when the unloading rate increased from 0.1 to 0.25 kPa/min, while the failure strength of the soil increased relatively less when the unloading rate increased from 0.25 to 2.5 kPa/min.

A linear relationship was determined between the undrained shear strength and the unloading rate. Under the same unloading path, the soil unloading strength increased with the unloading rate, and the cohesion varied significantly with an increase in the unloading rate; however, the internal friction angle did not vary significantly. The cohesion and internal friction of clay do not work simultaneously. Cohesion is characterized by brittle properties and can reach its maximum value under a small strain, whereas internal friction can only be fully exerted after considerable deformation has occurred. Moreover, the cohesion and internal friction exerted different degrees under different strain conditions, which were controlled by the shear rate. In addition, there may be differences in the strain between the cohesion and internal friction that fully functioned under different shear rate conditions. When the unloading rate is small (e.g., 0.1 kPa/min), the cohesion and internal friction of the soil act synchronously in a smaller proportion, and the failure strength is lower. Moreover, when the unloading rate increases to a certain level (e.g., 0.25 kPa/min), the proportion of the cohesion and internal friction of the soil acting synchronously increases, and the soil in the shear process, must overcome the rotation, rolling, and displacement resistance of the particles in addition to overcoming the slippage between the particles, which leads to a greater increase in the failure strength. Moreover, with a further increase in the unloading rate (e.g., 2.5 kPa/min), although it is also necessary to overcome the particle rotation, rolling, and other resistances, the proportion of cohesion and internal friction acting synchronously decreases, and the degree of growth of the failure strength decreases.

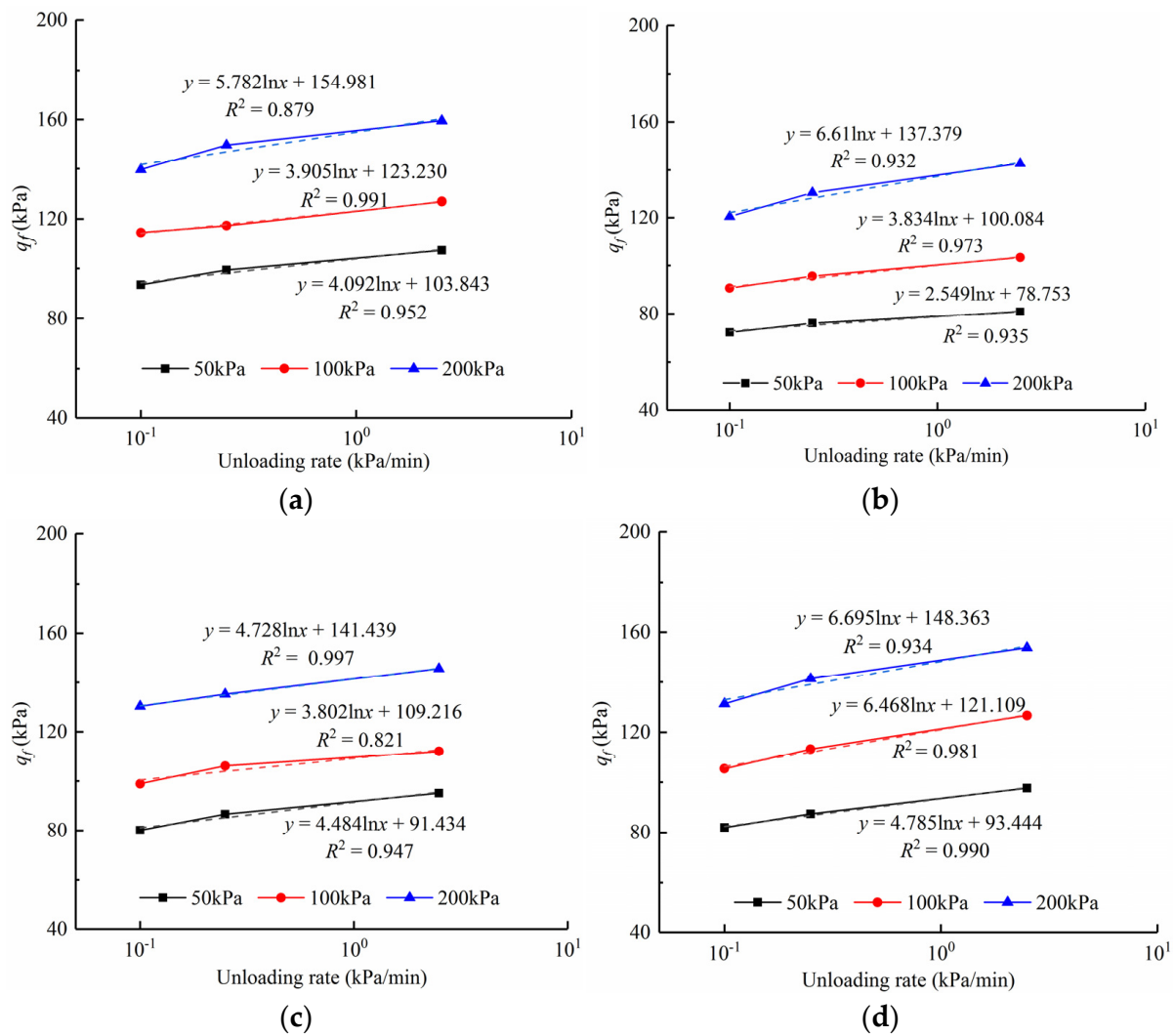


**Figure 19.** Relationship curves for the failure strength and unloading rate of specimens under different unloading paths. (a)  $CU_{-1.5}$ ; (b)  $UU_{1.0}$ ; (c)  $UC_{3.0}$ ; (d)  $UL_{\infty}$ .

To quantitatively describe the effect of the unloading rate on the undrained strength, we refer to the equation of the undrained shear strength unloading rate proposed by Li et al. [18], expressed as:

$$\rho_{q_{a0}} = \frac{\frac{\Delta S_{u0}}{S_{u0}}}{\Delta(\lg \dot{q}_a)} \times 100\% \quad (1)$$

where  $\dot{q}_{a0}$  is the reference unloading rate (here,  $\dot{q}_{a0} = 0.1$  kPa/min);  $\rho_{q_{a0}}$  is the unloading rate parameter under the reference unloading rate  $\dot{q}_{a0}$ ;  $S_{u0}$  is the undrained shear strength under the reference unloading rate  $\dot{q}_{a0}$ ;  $\Delta S_{u0}$  represents the increase in undrained strength corresponding to the increase in the unloading rate  $\Delta(\lg \dot{q}_a)$  in logarithmic coordinates.

The calculated results for unloading rate parameter  $\rho_{0.1}$  under different unloading paths are shown in Table 5. For the consolidation pressures of 50, 100, and 200 kPa,  $\rho_{0.1}$  under the  $CU_{-1.5}$  passive compression path is 6.09%, 4.22%, and 2.92%, respectively, and the average value is 4.41%. Meanwhile, the average values of  $\rho_{0.1}$  under the  $UU_{1.0}$ ,  $UC_{3.0}$ , and  $UL_{\infty}$  passive tensile paths and different consolidation pressures are 5.68%, 6.06%, and 9.06%, respectively. This indicates that the change in the unloading rate had a greater effect on the undrained strength under the passive tensile path than under the passive compression path.

**Table 5.** Shear test results for specimens under different unloading paths.

Unloading Stress Path	$\sigma_0/\text{kPa}$	Unloading Rate $v/\text{kPa}\cdot\text{min}^{-1}$	Failure Strength $qf/\text{kPa}$	Unloading Rate Parameter $\rho_{0.1}/\%$	$S_u/\sigma_0$
CU <sub>-1.5</sub>	50	0.1	93.58	6.09	0.94
	50	0.25	99.36		0.99
	50	2.5	107.25		1.07
	100	0.1	114.59	4.22	0.57
	100	0.25	117.33		0.59
	100	2.5	126.19		0.63
	200	0.1	139.71	2.92	0.35
	200	0.25	143.95		0.36
	200	2.5	149.50		0.37
UU <sub>1.0</sub>	50	0.1	72.26	4.95	0.72
	50	0.25	76.09		0.76
	50	2.5	80.84		0.81
	100	0.1	93.17	5.90	0.47
	100	0.25	100.48		0.50
	100	2.5	106.36		0.53
	200	0.1	120.01	6.20	0.30
	200	0.25	130.52		0.33
	200	2.5	137.87		0.34
UC <sub>3.0</sub>	50	0.1	80.12	7.82	0.80
	50	0.25	86.60		0.87
	50	2.5	95.15		0.95
	100	0.1	98.88	5.13	0.49
	100	0.25	105.94		0.53
	100	2.5	111.05		0.56
	200	0.1	130.32	5.23	0.33
	200	0.25	140.09		0.35
	200	2.5	146.68		0.37
UL <sub>∞</sub>	50	0.1	81.87	8.03	0.82
	50	0.25	87.43		0.87
	50	2.5	97.65		0.98
	100	0.1	105.37	9.62	0.53
	100	0.25	113.32		0.57
	100	2.5	129.70		0.65
	200	0.1	129.30	9.52	0.32
	200	0.25	146.39		0.37
	200	2.5	158.84		0.40

The relationship between the normalized undrained shear strength and the unloading rate was obtained by taking unloading paths CU<sub>-1.5</sub> and UU<sub>1.0</sub> as examples, as shown in Figure 20. As shown in the figure, the normalized shear strength under the unloading conditions is influenced by the stress path and unloading rate; thus, the mechanical parameters should be selected appropriately in the engineering design.

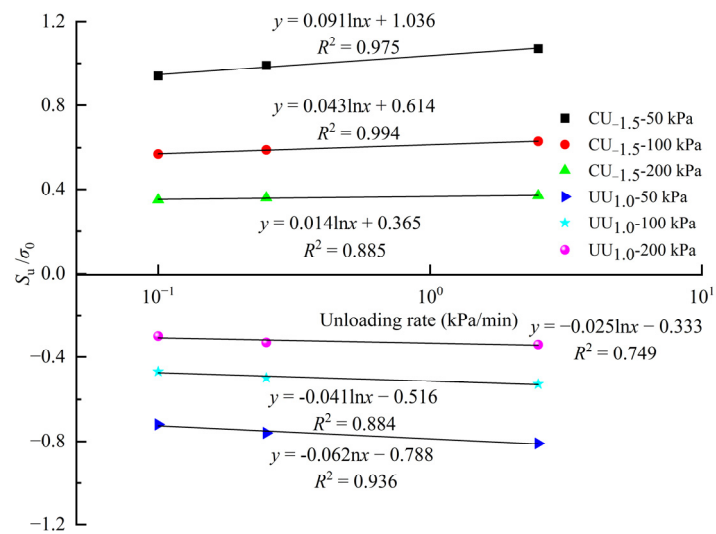


Figure 20. Relationship between normalized undrained shear strength and unloading rate.

#### 4. Microstructure Analysis

An FEI QUANTA 200 environmental scanning electron microscope was used to conduct scanning electron microscopy (SEM) tests near the shear bands of the undisturbed samples and samples after shear tests at different unloading rates. The specimen for the SEM tests was a cube of 10 mm × 10 mm × 10 mm. Before SEM was performed, a fresh section of the sample was sprayed with gold to increase the electrical conductivity. An image with a representative field-of-view was selected for each sample, as shown in Figure 21.

The SEM image of the undisturbed soil in Figure 21a shows curly lamellar mineral particles stacked in sheets. The structure of the Zhanjiang structured clay actually comprises a lamellar-stacked particle unit made of many single lamellae stacked together; specifically, a clay domain consisting of granular clastic minerals and a few monolithic clay mineral particles. The flattened lamellar pile and the single lamellar are dominated by edge–face contacts and edge–edge contacts, while a small amount of face–face contacts form a directional disorderly open flocculation structure. Additionally, the pores in the Zhanjiang structured clay existed mostly in the form of intergranular pores and a small number of isolated pores. The isolated pores were large and discontinuously distributed, mostly in the shape of circles or ellipsoids, whereas the intergranular pores appeared as sub-stable polygons.

From Figure 21b, it is clear that when specimens were shear damaged at the rate of 0.1 kPa/min, the arrangement between the basic units became closer due to the slow unloading rate. It is also apparent that the arrangement of soil particles maintained some lamellar single-sheet stacks, and some of the clay mineral aggregates broke into fine soil particles. Between the particles, there were mainly face–face contacts, a small number of edge–edge contacts, and the arrangement was not directional. Moreover, intragranular pores remained, and some of the pores gradually broke into smaller ones.

From Figure 21c, it can be seen that when the specimens were shear damaged at the rate of 0.25 kPa/min, with an increase in the unloading rate, the breakage of soil particles became more significant than that at 0.1 kPa/min, and the soil particles comprised a small number of lamellar forms and broken fine particles.

As shown in Figure 21d, when the specimens were shear-damaged at the rate of 2.5 kPa/min, owing to the fast unloading rate, the soil skeleton of the specimen was rapidly destroyed by shearing. The flocculation structure in the natural state disappeared, replaced by the face-to-face and point-to-face contacts of the large-volume unit body, and the soil particles of the specimen became finer.

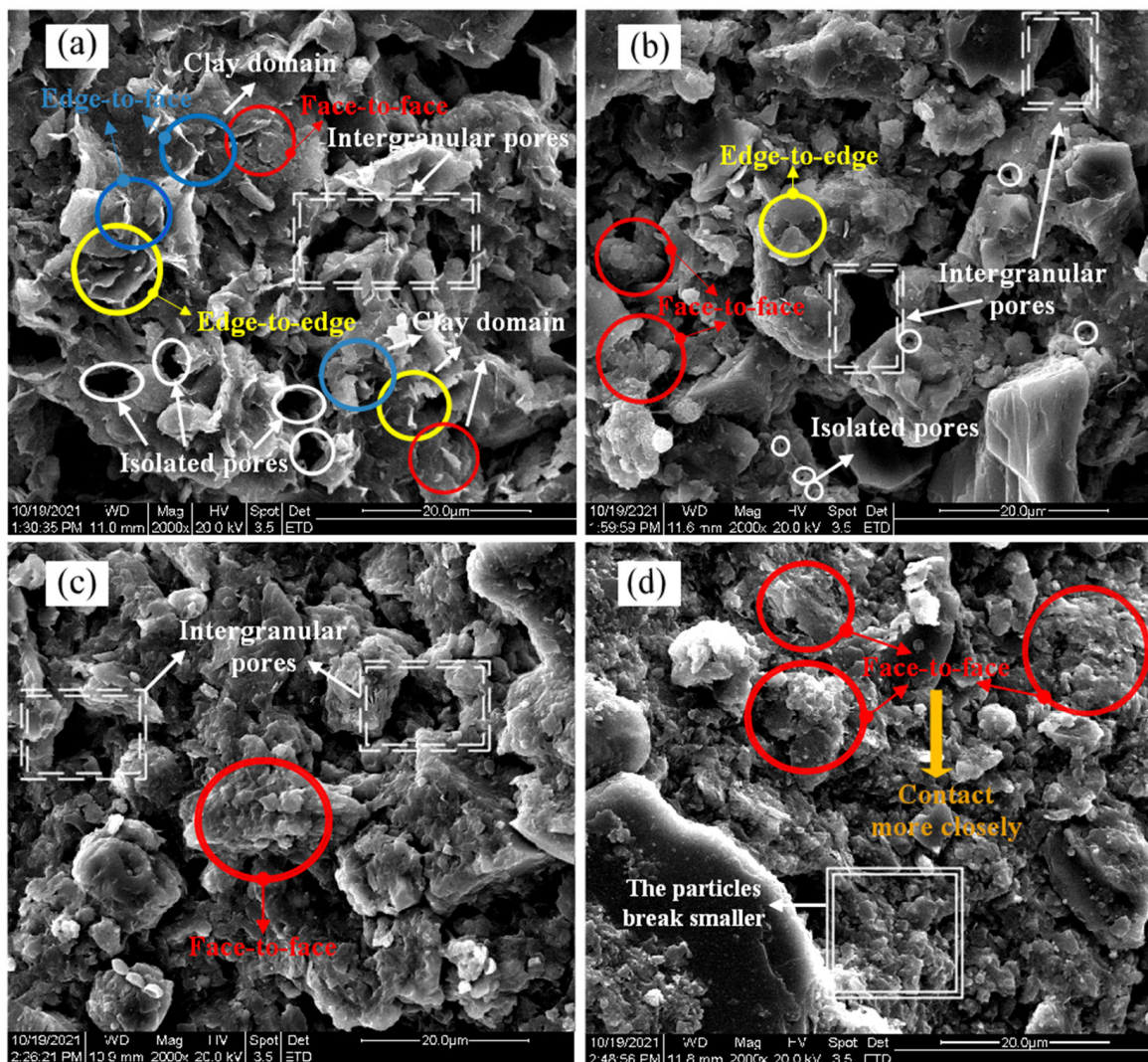


**Figure 21.** SEM images of specimens at different unloading rates under  $CU_{-1.5}$ ,  $\sigma_0 = 50$  kPa: (a) Undisturbed sample; (b) 0.1 kPa/min; (c) 0.25 kPa/min; (d) 2.5 kPa/min.

The microstructures of the Zhanjiang structured clay changed after shearing tests under different unloading rates, and the clay had no obvious sheet-pile-structured units owing to the destruction of connections, and the amount of intragranular pores decreased.

## 5. Conclusions

- The stress–strain relationship curves of the Zhanjiang structured clay exhibited strain softening under unloading states. Under the same axial strain, the greater the unloading rate, the greater the deviatoric stress. Under the same unloading path, the larger the confining pressure, the more significant the influence of the unloading rate on the soil. Moreover, the degree of deformation of the specimen under different unloading paths varied: the failure mode of the specimen under the  $CU_{-1.5}$  passive compression path was axial compression failure, while those of the specimens under the  $UU_{1.0}$ ,  $UC_{3.0}$ , and  $UL_{\infty}$  passive tensile paths were axial tensile failure.
- The pore water pressure characteristics of Zhanjiang structured clay are closely related to the unloading rate and unloading path. Under the  $CU_{-1.5}$  and  $UU_{1.0}$  unloading paths, the development of the pore water pressure with strain remained negative, and the effective stress path remained on the right side of the total path. While under the  $UC_{3.0}$  and  $UL_{\infty}$  unloading paths, the development of the pore water pressure of specimens significantly differed due to the influence of the confining pressure.

Furthermore, under the same conditions, the greater the confining pressure, the greater the peak pore water pressure, the smaller the unloading rate, the more fully the pore water pressure developed, and the greater the range of pore water pressure change. Therefore, during unloading construction, attention should be paid to engineering disasters caused by negative pore water pressure dissipation.

- The undrained shear strength of the Zhanjiang structured clay exhibited a semi-logarithmic linear increasing relationship with increasing unloading rate. Introducing unloading rate parameter  $\rho_{0.1}$ , the undrained strength under the CU<sub>-1.5</sub> passive compression path increased by 4.41% as the unloading rate increased from 0.1 to 2.5 kPa/min. The increases in undrained strength under the UU<sub>1.0</sub>, UC<sub>3.0</sub>, and UL<sub>∞</sub> passive tensile paths were 5.68%, 6.06%, and 9.06%, respectively. Thus, the influence of the unloading rate on the passive tensile paths is greater than that on the passive compression paths.
- The microstructure of the strong structured clay sample from Zhanjiang changed after shear tests at different unloading rates. The particle arrangement, contact relations, pore size, and shape varied to different degrees. During shearing, the Zhanjiang structured clay continuously self-adjusts its internal structure.

**Author Contributions:** L.L.: conceptualization, methodology, data curation, and writing—original draft. M.Z.: conceptualization, methodology, writing—review and editing, and investigation. R.Z.: methodology and investigation. H.L.: funding acquisition. All authors have read and agreed to the published version of the manuscript.

**Funding:** This work was funded by the National Natural Science Foundation of China (Grant No. 11802215) and the Natural Science Foundation of Hubei Province of China (Grant No. 2022CFA011), and the authors are grateful for this financial support.

**Data Availability Statement:** If readers require the data from this article, please contact the corresponding author.

**Conflicts of Interest:** The authors declare no conflict of interest.

## References

1. Huang, W.; Li, J.J.; Lu, Y.M.; Li, D.S.; Mou, Y.Q.; Wu, X.H.; Jiang, Z.J.; Li, Z.Y. Mechanical properties of soft soil considering the influence of unloading stress paths. *Adv. Civ. Eng.* **2021**, *2021*, 8813882. [[CrossRef](#)]
2. Huang, W.; Wen, K.J.; Li, J.J.; Fu, X.M.; Liu, S.H.; Li, Y.; Li, L.; Amini, F. Mechanical properties of soft soils experiencing lateral unloading under initial excess pore water pressure. *Arab. J. Geosci.* **2019**, *13*, 718. [[CrossRef](#)]
3. Han, J.; Yin, Z.Y.; Dano, C.; Hicher, P.Y. Effect of strain rate on the adhesive bond shearing resistance of stiff clay. *Transp. Geotech.* **2021**, *27*, 100479. [[CrossRef](#)]
4. Torisu, S.S.; Pereira, J.M.; De Gennaro, V.; Delage, P.; Puech, A. Strain-rate effects in deep marine clays from the Gulf of Guinea. *Géotechnique* **2012**, *62*, 767–775. [[CrossRef](#)]
5. Le, T.; Airey, D.; Standing, J.R. Influence of shearing strain rate on the mechanical behaviour of three structured clays. *Géotechnique* **2022**, 1–56. [[CrossRef](#)]
6. Lambe, T.W. Stress path method. *J. Soil Mech. Found.* **1967**, *93*, 268–277. [[CrossRef](#)]
7. Liu, G.B.; Hou, X.Y. Unloading stress-strain characteristics of soft soils. *Tunnel Rail Transit.* **1997**, *2*, 16–23. (In Chinese)
8. Yan, S.W.; Zhang, J.J.; Tian, Y.H.; Sun, L.Q. Pore pressure characteristics in isotropic consolidated saturated clay under unloading conditions. *J. Mar. Sci. Tech.* **2016**, *24*, 3. [[CrossRef](#)]
9. Lim, A.; Ou, C.Y. Stress paths in deep excavations under undrained conditions and its influence on deformation analysis. *Tunn. Undergr. Sp. Tech.* **2017**, *63*, 118–132. [[CrossRef](#)]
10. Jia, M.C.; Luo, W.S.; Zhou, Y.H.; Zhao, S.; Zhang, Z. A model of undrained stress-strain curves considering stress path and strain softening. *Int. J. Geomech.* **2021**, *21*, 04021213. [[CrossRef](#)]
11. Huang, W.; Wen, K.J.; Liu, D.Y.; Dong, Q.; Li, J.J.; Li, Y.; Li, L. Experimental study on influence of excess pore water pressure and unloading ratio on unloading mechanical properties of marine sedimentary soft soils. *Ocean Eng.* **2020**, *195*, 106680. [[CrossRef](#)]
12. Buisman, A.S. Results of long duration settlement tests. In Proceedings of the 1st International Conference on Soil Mechanics and Foundation Engineering, Cambridge, UK, 22–26 June 1936; Volume 1, pp. 103–107.
13. Sheahan, T.C.; Ladd, C.C.; Germaine, J.T. Rate-dependent undrained shear behavior of saturated clay. *J. Geotech. Eng.* **1996**, *122*, 99–108. [[CrossRef](#)]
14. Whitman, R.V.; Richardson, A.M. Effect of strain-rate upon undrained shear resistance of a saturated remoulded fat clay. *Géotechnique* **1963**, *13*, 310–324. [[CrossRef](#)]

15. Zhu, J.G.; Yin, J.H. Strain-rate-dependent stress-strain behavior of overconsolidated Hong Kong marine clay. *Can. Geotech. J.* **2000**, *37*, 1272–1282. [[CrossRef](#)]
16. Wu, S.S.; Lok, T.; Xu, Y.W.; Wang, D. Rate-dependent behaviour of a saturated clay under different stress histories and  $K_0$  conditions. *Acta Geotech.* **2020**, *15*, 1501–1512. [[CrossRef](#)]
17. Cai, Y.; Kong, L.W.; Guo, A.G.; Tuo, Y.F. Effects of shear strain rate on mechanical behavior of Zhanjiang strong structured clay. *Rock Soil Mech.* **2006**, *27*, 1235–1240. (In Chinese)
18. Li, X.M.; Kong, L.W.; Guo, A.G. Experimental study of the influence of unloading rate on the shear mechanical properties of undisturbed expansive clay. *Rock Soil Mech.* **2019**, *40*, 3758–3766. (In Chinese)
19. Yang, A.W.; Yang, S.K.; Zhang, Z.D. Experimental study of mechanical properties of dredger fill under different unloading rates and stress paths. *Rock Soil Mech.* **2020**, *41*, 2891–2912. (In Chinese)
20. Song, F.N.; Huang, X.; Luo, T.T.; Zou, J.Q.; Fu, R. Strain energy evolution and damage characteristics of deep clay under different stress rates. *J. Cent. South Univ.* **2022**, *29*, 2005–2018. [[CrossRef](#)]
21. Zhang, X.W.; Wang, G.; Liu, X.Y.; Xu, Y.Q.; Kong, L.W. Microstructural analysis of pore characteristics of natural structured clay. *Bull. Eng. Geol. Environ.* **2022**, *81*, 473. [[CrossRef](#)]
22. An, R.; Kong, L.W.; Shi, W.Z.; Zhang, X.W. Stiffness decay characteristics and disturbance effect evaluation of structured clay based on in-situ tests. *Soils Found.* **2022**, *62*, 101184. [[CrossRef](#)]
23. Li, L.; Zang, M.; Zhang, R.T.; Lu, H.J. Deformation and strength characteristics of structured clay under different stress paths. *Math. Probl. Eng.* **2022**, *2022*, 9266206. [[CrossRef](#)]
24. Zang, M.; Kong, L.W.; Zhang, R.T.; Wang, W.W. Study on characteristics of shear modulus of Zhanjiang structured clay during triaxial shearing. *Geotech. Geol. Eng.* **2021**, *39*, 603–616. [[CrossRef](#)]
25. *ASTM D2216*; Standard Test Methods for Laboratory Determination of Water (Moisture) Content of Soil and Rock by Mass. American Society for Testing and Materials: West Conshohocken, PA, USA, 2019.
26. *ASTM D854*; Standard Method of Test for Specific Gravity of Soils. American Society for Testing and Materials: West Conshohocken, PA, USA, 2019.
27. *ASTM D4318*; Standard Test Methods for Liquid Limit, Plastic Limit, and Plasticity Index of Soils. American Society for Testing and Materials: West Conshohocken, PA, USA, 2017.
28. *ASTM D1586*; Standard Method of Test for Penetration Test and Split-Barrel Sampling of Soils. American Society for Testing and Materials: West Conshohocken, PA, USA, 2018.
29. *ASTM D2166*; Standard Method of Test for Unconfined Compressive Strength of Cohesive Soil. American Society for Testing and Materials: West Conshohocken, PA, USA, 2016.
30. Touiti, L.; Bouassida, M.; Van, I.W. Discussion on the Tunis soft clay sensitivity. *Geotech. Geol. Eng.* **2009**, *27*, 631–643. [[CrossRef](#)]
31. *ASTM D4767*; Standard Test Method for Consolidated Undrained Triaxial Compression Test for Cohesive Soils. American Society for Testing and Materials: West Conshohocken, PA, USA, 2020.

**Disclaimer/Publisher's Note:** The statements, opinions and data contained in all publications are solely those of the individual author(s) and contributor(s) and not of MDPI and/or the editor(s). MDPI and/or the editor(s) disclaim responsibility for any injury to people or property resulting from any ideas, methods, instructions or products referred to in the content.